Tentative links between thermal diffusivity and fire-retardant properties in poly(methyl methacrylate)–metal oxide nanocomposites

Blandine Friederich, Abdelghani Laachachi, Michel Ferriol, David Ruch, Marianne Cochez, Valérie Toniazzo

Tentative links between thermal diffusivity and fire-retardant properties in poly(methyl methacrylate)—metal oxide nanocomposites

Blandine Friederich [a,b], Abdelghani Laachachi [a,*], Michel Ferriol [b], David Ruch [a], Marianne Cochez [b], Valérie Toniazzo [a]

[a] AMS (Department of Advanced Materials and Structures), Centre de Recherche Public Henri Tudor, 66 rue de Luxembourg, BP 144, L-4002 Esch-sur-Alzette, Luxembourg
[b] LMOPS, ex-UMR CNRS 7132, Université Paul Verlaine Metz, Département Chimie de l'IUT de Moselle Est, 12 rue Victor Demange, BP 80105, F-57503 Saint-Avold Cedex, France

Possible relationships between fire-retardant properties and thermal diffusivity for poly(methyl meth-acrylate) (PMMA) filled by melt blending with titanium dioxide (TiO_2), alumina (Al_2O_3) and boehmite (AlOOH) were investigated for a better understanding of the mode of action of metal oxides as fire-retardants (FR) in PMMA. Fire-retardancy was measured with a cone calorimeter and thermal diffusivity (α) by Laser Flash Analysis (LFA). LFA measurements have shown that heat dispersion is higher with titanium dioxide and boehmite than with alumina despite a larger surface area. For thermal diffusivity, discrepancies between the different nanofillers were only visible from 10 wt% onwards. Thermal degradation of PMMA-oxide nanocomposites and their thermal diffusivity could be linked. Moreover, a bi-linear relationship between the peak of heat release rate (pHRR) and the average of heat release rate (AHRR) showed the occurrence of a barrier effect.

1. Introduction

It has been reported that, due to fire, approximately 12 persons are killed and 120 are severely injured in Europe every day. This has also a considerable impact on the environment in terms of destruction of substructures, production of toxic and/or corrosive compounds (CO, dioxins, HCN, polycyclic aromatic compounds…). Moreover the material losses associated with these claims represent 1% of GDP (Gross Domestic Product) [1]. Consequently, it is necessary to find solutions in order to limit these risks by designing new materials with enhanced flammability properties. Nowadays, many companies (building and civil engineering, transportation, cable-making, electro-technical devices…) are directly concerned by this topic. Buildings contain an increasingly significant heat load in the form of highly combustible polymeric materials aiming at replacing more traditional ones (wood, alloys, metals…) and improving our comfort (domestic furniture, carpets, toys, household and leisure electric components and data processing equipment…). Potential sources of fire also tend to grow with the multiplication of electric and electronic devices. The increasing sophistication of electronics (increasingly powerful and fast microprocessors) and miniaturization have as a consequence a stronger concentration of energy leading to an increased risk of specific overheating and thus, of component ignition and subsequent fire. Under these conditions, regulations impose the use of materials presenting thermal stability as well as efficient fire-retardant (FR) properties. In parallel, emissions of smoke must be low, neither opaque, nor toxic. This evolution towards a greater safety seriously limits the use of many materials and also involves the rejection of solutions largely used so far and, in particular, halogen-based flame-retardants. Moreover, the analysis of the various statistics on the estimation of plastic consumption (180 MT/year with a global annual growth rate of approximately 8%) shows the economical importance of this field and illustrates this worldwide industrial challenge [1].

In the present paper we focus on poly(methyl methacrylate) (PMMA). PMMA is an important thermoplastic material used for its transparency and rigidity, both in construction, lighting and electronics, but its major drawback is its flammability (limiting oxygen index (LOI) equal to 18). Recent studies [2,3] have shown that the incorporation of organoclays and phosphorus compounds, among others, improve the fire-retardancy of polymers and especially of PMMA. Moreover metallic oxides improve both PMMA thermal stability and fire-retardancy [3,4] making it a good candidate for

* Corresponding author. Tel.: +352 42 59 91 591; fax: +352 42 59 91 555.
E-mail address: abdelghani.laachachi@tudor.lu (A. Laachachi).

synergy effects with conventional fire-retardants. An increase of the thermal stability between about 25 °C and 40 °C for 5–20 wt% of antimony oxide (Sb_2O_3) in PMMA was demonstrated by thermogravimetric analysis (TGA) in air [5]. Furthermore the incorporation of 15 wt% oxide led to a significant stability increase of the polymer: the effect was more pronounced in the case of titanium dioxide (TiO_2) compared to alumina (Al_2O_3) with a temperature shift close to 60 °C at half degradation (50% weight loss). Besides, flame behaviour was improved since the time-to-ignition (TTI) was increased and the peak of heat release rate (pHRR) was reduced [6]. But in order to get relevant fire-retardant properties it was necessary to add high filler content in the polymer (close to 15 wt%). This raises the question of the impact of such high loadings on the mechanical properties of PMMA.

Therefore the first aim of this study is to investigate the impact of the incorporation of nanoparticles into PMMA on its mechanical properties (we will focus on Young's modulus). In a second step, we have studied the impact of different nanofillers loadings (2–15 wt% TiO_2, Al_2O_3 and boehmite (AlOOH)) on the heat transfer in PMMA. The measurement of thermal transfer in the nanocomposites was performed by Laser Flash Analysis (LFA). The obtained results enabled us to suggest probable relationships which might exist between fire-retardant properties measured by cone calorimetry and thermal diffusivity. We are aware that combustion is a complex phenomenon and in the present state of the work, it seems difficult to generalize these results to other polymer composites. However, this approach is rather original since, to our knowledge, it has rarely been attempted in other systems.

2. Materials

PMMA (Acrigel® DH LE, M_w = 78,000 g mol^{-1} based on GPC analysis) was purchased from Unigel Plàsticos.

Three different types of nanometric fillers were used: titanium dioxide (TiO_2), alumina (Al_2O_3) and boehmite (AlOOH). Nanometric titanium oxide (Aeroxide® TiO_2 P25) and alumina (Aeroxide® Alu C), with respective median particles size equal to 21 and 13 nm and specific surface areas equal to 50 and 100 m^2 g^{-1}, were provided by Evonik Degussa GmbH. Further information is available in Table 1.

Boehmite (Actilox® 400SM) was donated by Nabaltec (D_{50} = 0.35 μm and specific surface area: 40 m^2 g^{-1}) and was used for mechanical tests and thermal conductivity measurements. Its features are presented in Table 2. For fire tests by cone calorimetry, a boehmite with similar particles size (Apyral AOH 180 from Nabaltec) was used.

3. Nanocomposites preparation

PMMA and nanoparticles were blended by melt compounding in a 15 cm^3 co-rotating twin-screw DSM Xplore micro-compounder at 230 °C and at 200 rpm during 4 min, under inert atmosphere (argon). Different nanoparticles loadings were used (2, 5, 10, 15 wt% and additionally 20 wt% in some cases). Prior to extrusion, all the materials were dried in an oven at 80 °C for at least 4 h.

Table 1
Characteristics of nanometric TiO_2 and Al_2O_3 (Evonik-Degussa).

Specifications	Aeroxide® TiO_2 P25	Aeroxide® Alu C
Average particle size (nm)	21	13
BET specific surface area ($m^2 \cdot g^{-1}$)	50 ± 15	100 ± 15
TiO_2 (%)	≥99.5	≤0.1
Al_2O_3 (%)	≤0.3	≥99.6
SiO_2 (%)	≤0.2	≤0.1
Fe_2O_3 (%)	≤0.01	≤0.2
HCl (%)	≤0.3	≤0.5

Table 2
Characteristics of AlOOH (Nabaltec).

Specifications	Actilox® 400SM
D_{10} (μm)	0.2
D_{50} (μm)	0.35
D_{90} (μm)	0.5
BET specific surface area ($m^2 \cdot g^{-1}$)	40
AlOOH (%)	98.7

4. Characterization

4.1. Morphology of nanocomposites

The degree of dispersion of nanofillers in the PMMA matrix was ascertained using transmission electron microscopy (TEM). TEM observations were performed with a Hitachi H800 MT at 200 kV. The samples were 70 nm thick and were prepared with a LEICA EM FC6 cryo-ultramicrotome at 25 °C.

4.2. Mechanical properties

The evaluation of the mechanical properties of PMMA and its nanocomposites was carried out using a Dynamic Mechanical Analyzer (DMA 242C-Netzsch). Storage (E') and loss (E'') moduli were measured as a function of temperature (−50 °C to +160 °C) with a dynamic temperature ramp sweep at 2 °C·min^{-1}. Measurements were performed using the single cantilever bending mode at a frequency of 1 Hz. The storage modulus or Young's modulus is the elastic response to deformation, whereas the loss modulus is the viscous response corresponding to the energy lost through the material movement. The damping factor (tan δ) was deduced from these measurements applying equation (1):

$$\tan\delta = \frac{E''}{E'} \quad (1)$$

From the tan δ curve, DMA allows an accurate determination of the glass transition temperature (Tg), even for loaded samples. All the DMA specimens were pressed and cut into a 35 mm-long, 9.9 mm-wide and 2.5–2.6 mm-thick sample. To ensure a consistency in the data 3–4 specimens were tested for each formulation.

4.3. Thermal properties

4.3.1. Thermal diffusivity measurement

The thermal diffusivity of PMMA and its nanocomposites was measured from room temperature to 170 °C using a laser flash technique (Netzsch LFA 457 Microflash™) under inert atmosphere (argon flow: 100 mL·min^{-1}). This technique was introduced by Parker et al. [7] in 1961. The schematic design of the apparatus is shown in Fig. 1.

It consists of:

- a Nd-glass-laser, with a maximum pulse energy of 15 J and a pulse length of 0.33 ms, based in the bottom part of the device;
- a furnace for a controlled heating of the samples;
- a Mercury Cadmium Telluride IR-detector coupled to an InSb detector located on the top part of the instrument.

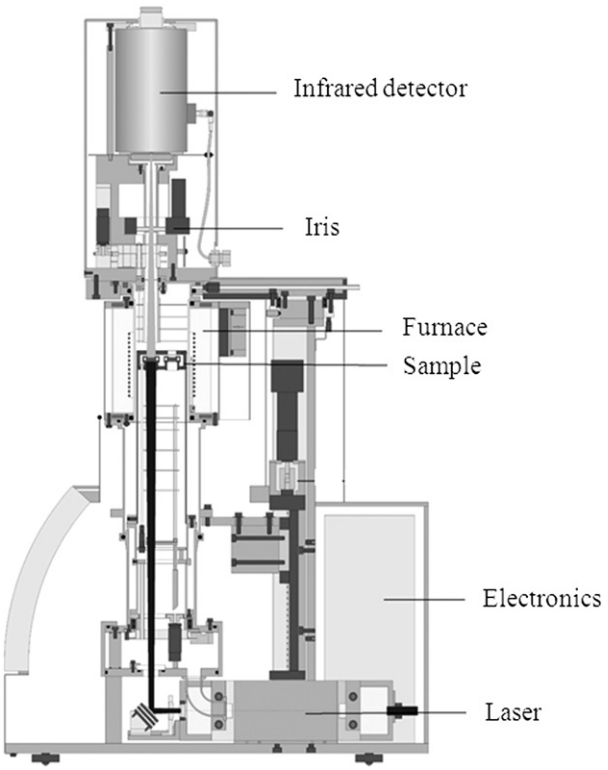

Fig. 1. Schematic view of Netzsch LFA 457 Microflash™ [8].

Samples were plane and parallel disks with 12.7 mm in diameter and about 1.1 mm thick. Owing to the PMMA translucency, prior to measurements, graphite was sprayed on both sample surfaces to avoid the penetration of the laser light through the sample and to improve the signal-to-noise ratio of the infrared detector signal. Graphite was also used due to its high thermal diffusivity, allowing the propagation of heat through the samples. Their front side is heated by a short laser pulse (0.5 ms). The heat induced propagates through the sample and causes a temperature increase on the rear surface. This temperature rise is measured versus time using the IR-detector. The thermal diffusivity is then determined using the "half-rise-time" ($t_{1/2}$) corresponding to the time for the back face temperature to reach 50% of its maximum value and for which $\omega = 1.38$. The thermal diffusivity can be calculated using equation (2):

$$\alpha = \frac{1.38 \cdot L^2}{\pi^2 \cdot t_{1/2}} \tag{2}$$

where L is the specimen thickness. Preliminary measurements of the expansion coefficient of PMMA and of its nanocomposites were performed on a DIL 402C-dilatometer (Netzsch). In the studied temperature range (25 °C–170 °C), that coefficient was low enough to be neglected.

For each sample and condition, measurements were repeated three times in order to collect meaningful data between room temperature and 170 °C. Radial and facial heat losses, finite pulse time effects and internal radiative heat transfer were taken into account using advanced mathematical regression routines, like Taylor-Clark or Cowan models for example, provided by the software [8,9].

Laser Flash Analysis is a direct measurement method for measuring thermal diffusivity and an indirect one for measuring thermal conductivity. This technique offers numerous advantages including:

- independence of heat flow and temperature gradient on the equation for thermal diffusivity calculation;
- quick data acquisition;
- heat losses corrected by models;
- few amount of material necessary for preparing samples.

4.3.2. Thermal conductivity determination

Thermal conductivity (k) can be determined using equation (3):

$$k(T) = \alpha \cdot C_p \cdot \rho \tag{3}$$

where C_p is the heat capacity determined by Differential Scanning Calorimetry and ρ is the density measured with a densimeter. Both devices are described hereinafter.

4.3.2.1. Differential Scanning Calorimetry (DSC). DSC scans were recorded on a Differential Scanning Calorimeter 204 F1 Phoenix® (Netzsch) in inert atmosphere (nitrogen), in the temperature range 25 °C–180 °C with a heating rate of 10 °C·min^{-1}. The powdered samples (20–25 mg) were placed into alumina crucibles. The heating was repeated twice to avoid parasitic phenomena beside the glass transition temperature (Tg) when calculating the heat capacity (C_p). C_p was calculated on the second cycle.

4.3.2.2. Density measurements. Densities of the PMMA-based nanocomposites were measured with a Wallace High Precision Densimeter X21B and were compared to theoretical values using equation (4):

$$\frac{1}{\rho_M} = \frac{W_p}{\rho_p} + \frac{W_c}{\rho_c} \tag{4}$$

where W is the weight fraction and ρ the density (the subscript p refers to the polymer and c to the filler).

4.3.3. Thermal analysis

Thermogravimetric analyses (TGA) were performed with a Mettler-Toledo TGA/SDTA 851e thermobalance operating in air environment under gas flow of 65 cm^3·min^{-1} in alumina crucibles (150 μL) containing 20–25 mg of sample. The runs were carried out in dynamic conditions at the constant heating rate of 10 °C·min^{-1}.

4.3.4. Flammability

Flammability properties of PMMA-based nanocomposites were studied by cone calorimetry (Fire Testing Technology). 100 × 100 × 4 mm^3 sheets were exposed to a radiant heat flux of 35 kW·m^{-2}. The principle of the device is based on a study of Huggett [10] who verified that for organic matter the heat released is proportional to the amount of oxygen consumed.

5. Results and discussion

5.1. Morphology

TEM analyses of the PMMA-oxides nanocomposites were performed in order to investigate the dispersion and the distribution of oxide nanoparticles into the PMMA. Fig. 2 shows some typical micrographs obtained.

Although no surface treatment was applied, metal oxides are well dispersed in the matrix with a slight tendency to aggregation.

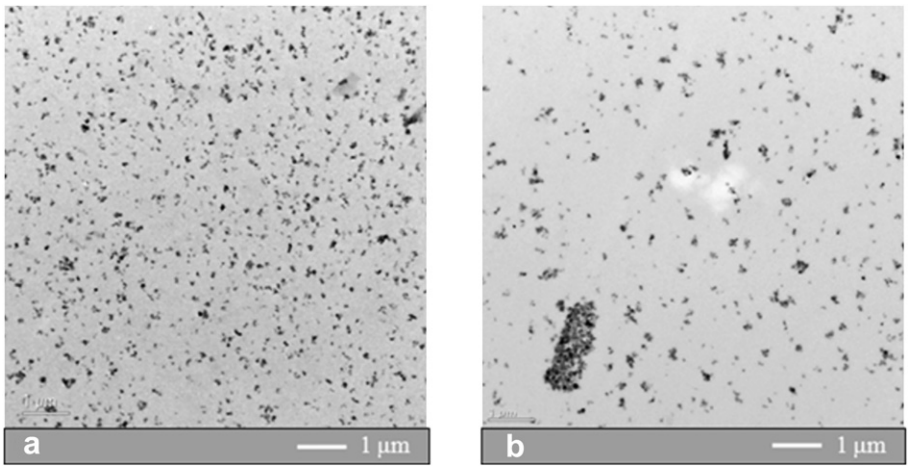

Fig. 2. TEM micrographs of (a) PMMA-5 wt% Al_2O_3 and (b) PMMA-5 wt% TiO_2.

5.2. Thermo-mechanical properties

Since metal oxides can be used for improving both thermal stability and fire properties of PMMA, it is important that they do not dramatically deteriorate the polymer mechanical properties (rigidity). Fig. 3 shows the effect of metal oxides nanoparticles on mechanical properties (storage modulus E') obtained by DMA measurements. The storage modulus connects with the elastic modulus of the materials.

At room temperature, PMMA exhibits a high storage modulus ($E'_{25°C} = 2534 \pm 68$ MPa). The addition of 2–5 wt% nanoparticles undergoes a slight decrease of E' with a maximum loss of the storage modulus between 14 and 20%, depending on the nature of the nanoparticles, followed by an increase as more nanofillers are added to the matrix until regaining the modulus value of PMMA. The major information emerging from these measurements is that the addition of nanofillers like TiO_2, Al_2O_3 and AlOOH has little effect on the material at 10–15 wt%.

The damping factor (tan δ) was also measured by DMA by calculating the ratio of the loss modulus E'' and storage modulus E' (see equation (1)). The damping factor measures the damping of vibrations during a dynamic deformation. The temperature for which that ratio reaches a maximum value corresponds to the glass transition temperature (Tg) (Fig. 4).

Tg tends to increase with the filler loading content except for Al_2O_3. For each composition, one can note a 5% maximum rise for Tg when compared to the neat polymer ($Tg_{PMMA} = 118.6$ °C). Tg values obtained by DSC (not shown) were, on an average, slightly lower than those determined by DMA (a maximum increase of 2 °C compared to neat polymer), but followed the same trend. Particles size, shape, volume fraction and dispersion play a very important role on nanocomposites mechanical behaviour [11]. Indeed a good particles' dispersion allows them to interact with a large volume of polymer. Moreover it has been shown elsewhere that the interaction depends on the specific surface area of particles. The interaction is all the more important than the specific surface area is high. Thus, well dispersed nanoparticles interact with a larger volume of the polymer than micrometric ones.

Filler–matrix interactions can also significantly affect the composite properties [12]: the storage modulus usually increases with increasing volume fraction in the case of good interaction. A decreasing particle size also generally leads to an increase of the modulus of elasticity. In their paper, Jordan et al. [12] listed the mechanical properties (elastic modulus, yield stress, ultimate stress, strain-to-failure) for different composites based on polymer. For each composite, they presented the quality of the interaction at the filler–matrix interface (good/poor). Nevertheless, no universal

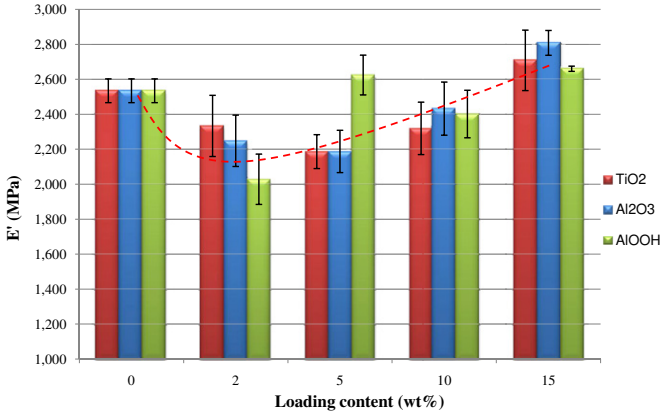

Fig. 3. Storage modulus at 25 °C for PMMA and its nanocomposites versus the oxide loading content.

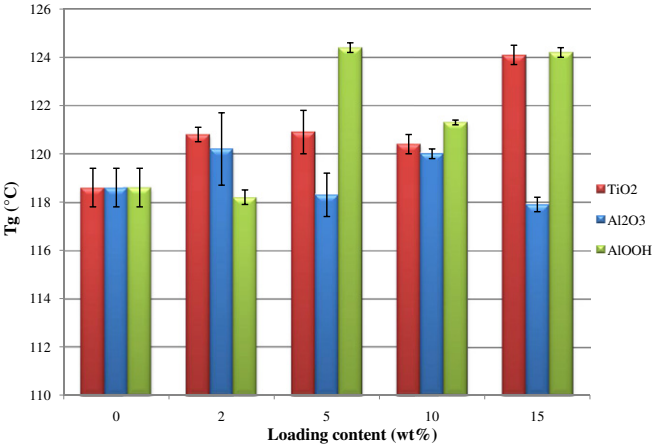

Fig. 4. Glass transition temperature for PMMA and its nanocomposites versus the loading.

patterns could be deduced between the mechanical properties and the quality of the interface for polymer nanocomposites.

Interesting results were obtained by Ash et al. [13] who performed DMA analysis on a PMMA–Al_2O_3 system. Their results showed a poor interface interaction between PMMA and alumina nanoparticles, characterized by a sharp drop of E' followed by a steady increase, as more nanofiller was added to the polymer. Even 10 wt% filler could not help recovering the Young's modulus of the pure system. This trend was similar to that obtained for our nanocomposites, except that the drop in E′ was not so important and that the elastic modulus of the pure system was recovered at 10–15 wt% depending on the nanoparticles. Ash attributed the drop of E' to the lowering of Tg. The decrease in Tg, due to weak polymer–particles interactions, was explained by the formation of cracks visible by microscopy. No decrease in Tg was observed during our study; on the contrary, an increase up to 6 °C was recorded as the loading increased which can reveal the presence of a zone of restricted motion of polymer chains around the particles [5]. Polymer chain mobility restriction can have two reasons [14]: (i) adsorption of polymer on the oxide surface (chemical bonding); (ii) steric hindrance due to the particles (physical reason). Chemical adsorption of poly(methyl methacrylate) on the oxide surface is done according to the mechanism proposed by Laachachi et al. in the Ref. [15]: PMMA methoxycarbonyl functional groups react with the –OH from the oxide surface, leading to a change of the degradation mechanism of PMMA in the presence of oxides (production of methanol, methacrylic acid and propanoic acid methyl ester).

Composite theory predicts that improved bonding between the matrix and reinforcing phase leads to improved mechanical properties [16,17]. However, mechanical tests of nanocomposites have shown mixed results, because good mechanical properties can only be achieved by uniform and efficient load transfer through a strong bond at the filler–polymer interface [18]. But it is important to have a uniform bonding on a fine scale rather than locally unevenly strong bonds, since areas of the interface which are not in contact behave as cracks under applied stress. However, at the molecular level, an interface is not fully continuous, making intermolecular interactions in an intermittent manner. An interphase region, which thickness depends on the nature of interactions between the filler and the polymer chains, then forms inevitably as depicted in Fig. 5.

Ciprari et al. [19] suggested that the bonding between PMMA and alumina nanoparticles surface happens as follows: –OH groups form on alumina surface through atmospheric water vapour (5):

$$Al_2O_3 \leftrightarrow 2AlO(OH) \quad (5)$$

Hydrolysis of PMMA ester groups follows, leading either to –COOH groups or to its conjugate $-COO^-$ base group according to reaction (6):

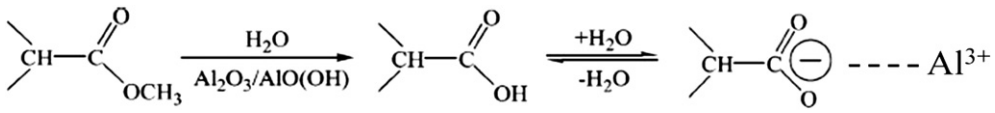

(6)

The $-COO^-$ group reacts with charged Al(III) atoms promoting the formation of a bond between PMMA and the alumina nanoparticles surface.

A weak interaction of polymer chains with the surface of oxide particles leads to the formation of an interphase characterized by a large thickness and polymer chains in the form of loops extending into the matrix, which can explain the low density of that region (Fig. 5a). This low density interphase somehow weakens the material since nanoparticles have a high surface/volume ratio. On the contrary, strong interactions are characterized by an interphase with low thickness and density, because the loops are of low amplitude (Fig. 5b) [11,19,20]. TEM micrographs clearly show this interphase (Fig. 6). It corresponds to the white layer surrounding the nanoparticles and the aggregates.

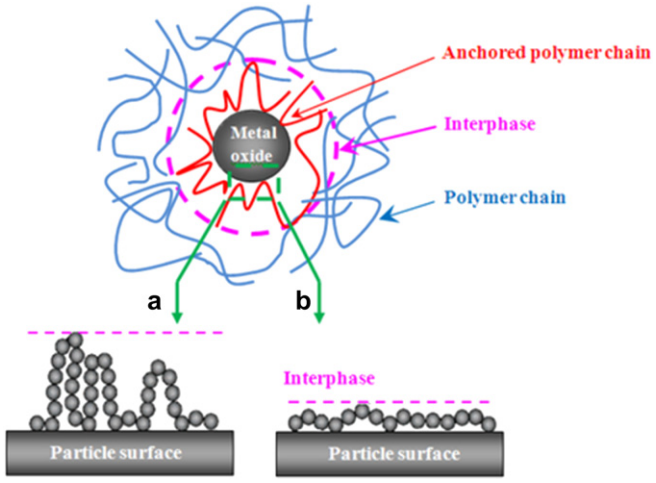

Fig. 5. Nature of the adsorption of polymer chains onto the metal oxide surface: (a) Weak bonding, (b) Strong bonding [19,20].

Generally, an increase of Tg is accompanied by a strengthening of the material and thus the increase of E' [13]. However, we measured both an increase of Tg and a depletion of E'. We can infer the existence of an interphase as presented in Figs. 5 and 6 leading to the decrease of the storage modulus. The increase observed from 5 to 10 wt% could come from the Tg increase, which would counterbalance the action of the interphase. Indeed, the interphase would tend to reduce E', whereas an increase in Tg (observed by DSC and DMA) would tend to increase E'. From a given loading content, the effect of Tg would take better on that of the interphase resulting in an increase of E'.

5.3. Fire-retardancy

The cone calorimeter is one of the most effective bench scale methods for investigating combustion properties of polymer materials. Various parameters can be measured with that device, but we have focused on time-to-ignition (TTI), total heat released (THR), heat release rate (HRR) and its peak (pHRR). Cone calorimeter tests were carried out with the following loadings: 0, 5, 10 and 15 wt%. When relevant, results for 20 wt% filler are also presented. For cone calorimeter data, standard deviation was 5%. Fig. 7 presents the change of TTI as a function of nanofillers content.

Adding nanofillers to PMMA led to an increase of TTI of up to 22% for 15 wt% filler. Two factors can be invoked: (i) increase of the

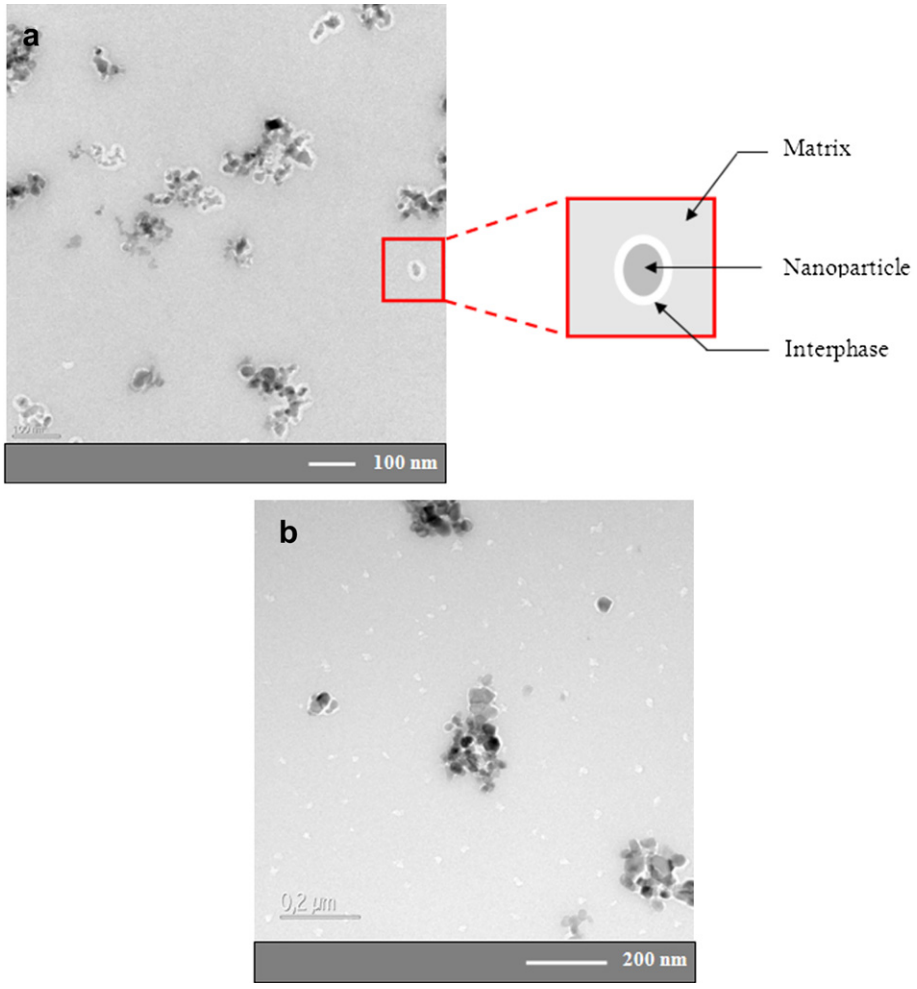

Fig. 6. TEM micrographs of (a) PMMA–5% Al_2O_3 and (b) PMMA–5% TiO_2 showing the interphase surrounding the aggregates and the particles.

thermal stability of the polymer in the presence of oxides, confirmed by thermogravimetric analysis, (ii) increase of the thermal diffusivity of samples when adding metal oxides [6].

Heat release rate (HRR) is the measure of the amount of heat released by a material per unit area when exposed to a fire radiating at constant heat flux. This variable varies with exposure time as the composite is progressively burned. According to Babrauskas and Peacock [21] even though fire deaths are primarily caused by toxic gases, the HRR has been found to be one of the most important parameters to predict fire hazard (maximum temperature and flame spread rate). Its maximum is named peak of heat release rate (pHRR) and it generally arises over a short period of time. pHRR can also be viewed as the "driving force" of the fire [21]. Thus, pHRR is a tremendous help to evaluate fire safety [22,23]. Fig. 8 presents the changes of pHHR with nanofiller content.

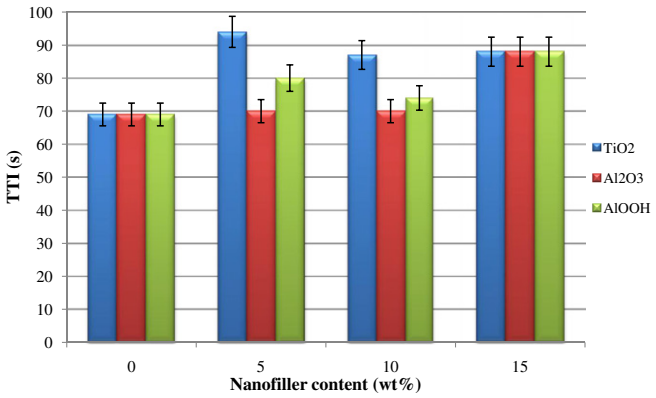

Fig. 7. TTI versus nanofillers content for PMMA, PMMA–TiO_2, Al_2O_3 and AlOOH nanocomposites.

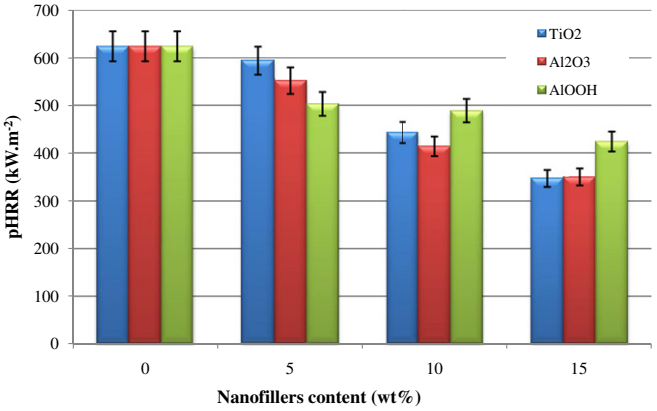

Fig. 8. pHRR versus nanofillers content for PMMA, PMMA–TiO_2, Al_2O_3 and AlOOH nanocomposites.

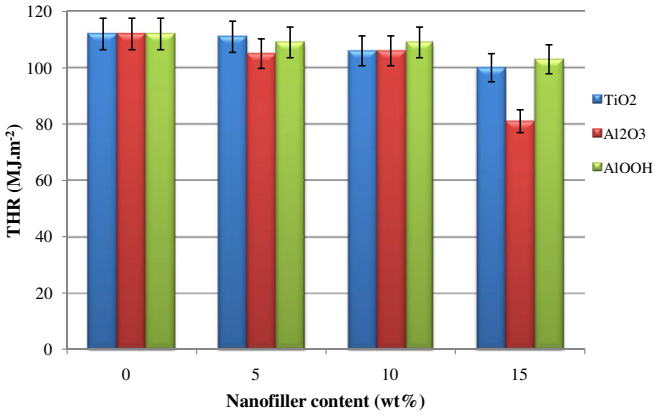

Fig. 9. THR versus nanofillers content for PMMA, PMMA–TiO_2, Al_2O_3 and AlOOH nanocomposites.

The addition of nanoparticles to PMMA leads to a decrease of pHRR: 15 wt% of boehmite caused a 32% decrease and the two other fillers were more effective in causing a fall of 46%.

Fig. 9 presents the change of THR as a function of nanofiller content.

The addition of oxide nanoparticles to PMMA causes a small decrease of THR. 15 wt% alumina led to a 28% decrease of THR. But in the case of organo-modified montmorillonite (OMMT), it has been reported that the addition of OMMT did not help to diminish the THR, whereas the pHHR could be reduced (sometimes by more than 50% compared to virgin polymer).

From the cone calorimeter experiments, the presence of oxide suggests a change of the PMMA degradation mechanism. According to the literature, metal oxides act on different levels:

- In the gas phase, metal oxides inhibit radical reactions of flame spread and thus they are at the origin of the slowdown of the combustion reaction. Active radicals HO• being adsorbed on the surface of particles, a part of the collision energy is transferred to the oxide which forms HOO• radicals less reactive than the initial HO• [24].
- Metal oxides also act in the condensed phase by migrating to the surface of the sample. In this way, they form a physical barrier preventing the migration of decomposition products from the bulk to the outside of the sample. The barrier also prevents the diffusion of oxygen to the surface of the sample, slowing down the propagation of fire.
- Boehmite can decompose endothermically into Al_2O_3 according to reaction (7):

$$2\,\mathrm{AlOOH} \xrightarrow{\Delta} \mathrm{Al_2O_3} + \mathrm{H_2O} \qquad (7)$$

The water released dilutes the fuel supply in the gas phase slowing down the decomposition [25].

- The presence of particles with different intrinsic thermal diffusivities modifying the heat transfers through the material was suggested by Laachachi et al. [6]. This was considered by these authors for giving a possible explanation to the increase in thermal stability. In the present study, we have deepened that aspect by attempting to draw a parallel between fire-retardancy

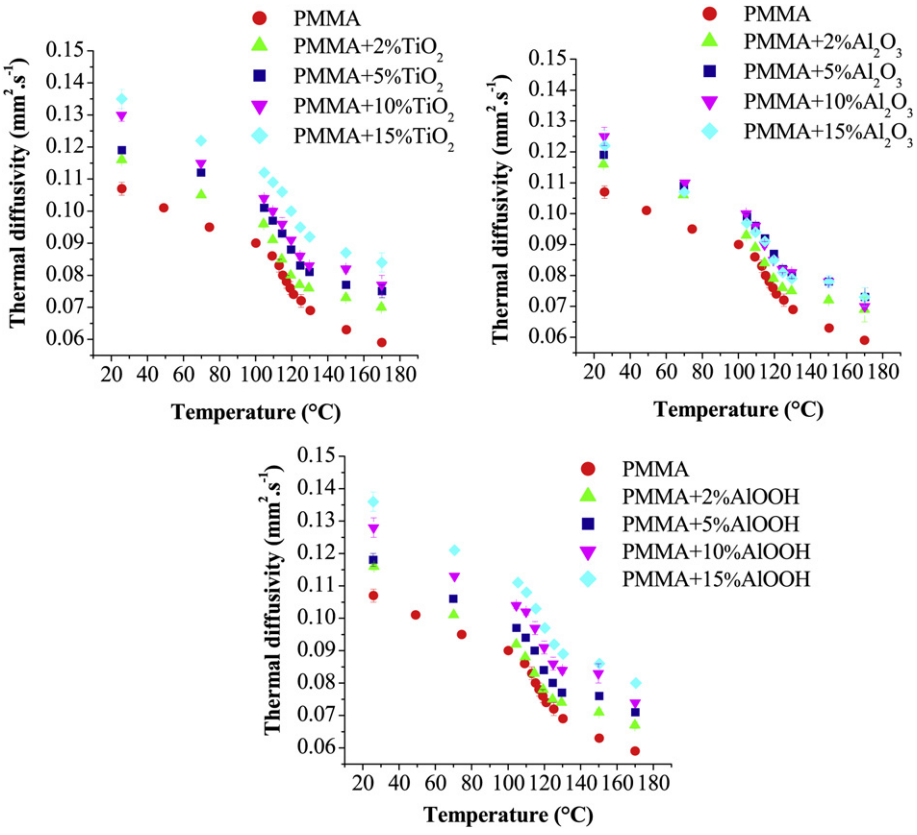

Fig. 10. Thermal diffusivity as a function of temperature for PMMA–TiO_2, PMMA–Al_2O_3 and PMMA–AlOOH nanocomposites.

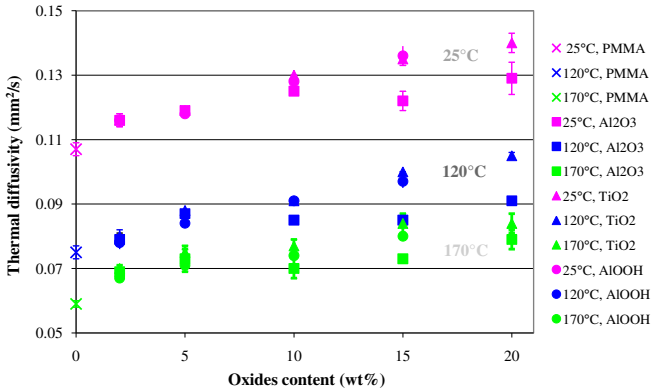

Fig. 11. Thermal diffusivity as a function of the nanoparticles content at 25 °C, 120 °C and 170 °C.

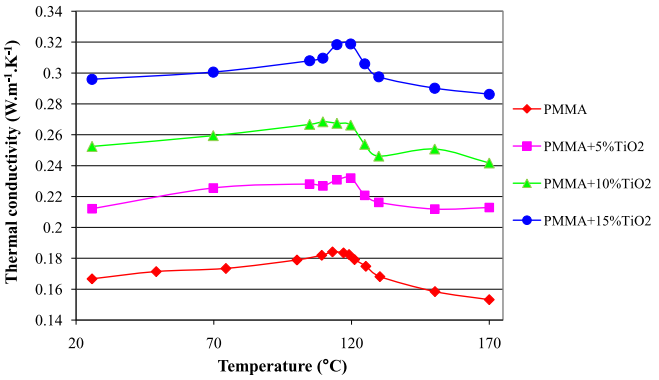

Fig. 12. Thermal conductivity as a function of temperature for PMMA–TiO_2 nanocomposites.

properties and thermal diffusivity measured for all the PMMA-oxide nanocomposites.

5.4. Thermal properties

Thermal diffusivity, denoted α, is the ability of a material to transmit heat rather than to absorb it. Investigating this intrinsic property will help to get a better knowledge about the impact of metal oxides on the thermal properties in composites and on fire-retardant properties. Measurements of thermal diffusivity of PMMA-oxide nanocomposites as a function of temperature are presented in Fig. 10.

Similar changes of thermal diffusivity were obtained whatever the metal oxide. Thermal diffusivity decreases with temperature and the decrease is speeding up around the glass transition temperature (Tg = 116 °C), following the increase in heat capacity of the composite. It means that the heat takes longer to pass through the material for temperatures above the Tg. In the studied temperature range (25 °C–170 °C), the thermal diffusivity of PMMA–TiO_2, Al_2O_3 and AlOOH systems is higher than that of pure poly(methyl methacrylate) and α increases with the filler content. At 25 °C, adding 15 wt% of TiO_2, Al_2O_3 and AlOOH led respectively to an increase of 26%, 14% and 27% of α compared to the reference (virgin PMMA). At 170 °C, the gap increases more, representing 42%, 24% and 36%. TiO_2 and AlOOH have a better ability to dissipate heat in PMMA than Al_2O_3, despite the fact that alumina exhibits the largest surface area (100 ± 15 $m^2 \cdot g^{-1}$). The differences in performance between fillers are only visible from 10 wt% as shown in Fig. 11.

A decrease of thermal diffusivity against temperature was also noted by Nunes dos Santos et al. in the case of PMMA [26], but the sharp fall was not highlighted because they limited their measurements to three temperatures. Thermal conductivity (k) can be inferred from thermal diffusivity by knowing the specific heat (C_p) and density of each material according to equation (3). The specific heat was measured by DSC. Densities of nanocomposites measured experimentally with a densimeter were very consistent with the theoretical values obtained with equation (4). The values of thermal conductivities calculated from this equation are presented in Fig. 12 for PMMA–TiO_2 nanocomposites.

The same behaviour was observed for PMMA–Al_2O_3 and PMMA–AlOOH nanocomposites. The thermal conductivity increases with the nanofiller content with the presence of a small peak around Tg, implying that the nanocomposite becomes less insulating. The small peak is also present for PMMA–Al_2O_3 nanocomposites, but the thermal conductivity curves of the different compositions overlap whereas being higher than for PMMA. This might come from the smaller gap between thermal diffusivity curves than for TiO_2 and AlOOH. In general, at the macromolecular level, effective heat transfer by conduction requires, on the one hand, material with high thermal conductivity and, on the other hand, good thermal contact between the two surfaces across which heat transfer occurs [27].

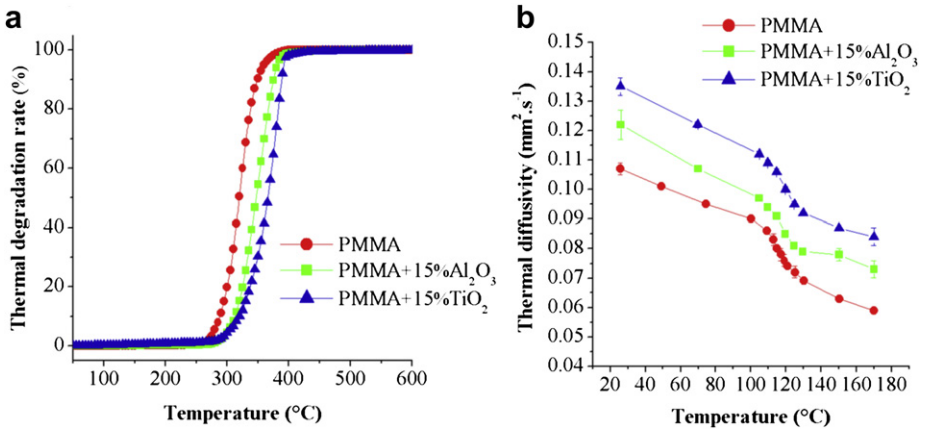

Fig. 13. (a) Reaction rate of the thermal degradation for PMMA, PMMA–15%Al_2O_3 and PMMA–15%TiO_2 nanocomposites under air (heating rate: 10 °C·min^{-1}); (b) Thermal diffusivity of PMMA, PMMA–15%Al_2O_3 and PMMA–15%TiO_2 versus temperature.

Thermal conductivity of multiphase materials is a function of the shape and size distribution of fillers, of the volume fractions of phases, of their topologies and intrinsic thermal conductivity [28]. In amorphous polymers, the heat transfer mode was presented by Oskotsky et al. [29] as taking place by inelastic dissipation of phonons located at the defaults. According to Bashirov et al. [30] the transfer would happen by a rise of the polymer free-volume when passing through Tg, because air has a low thermal diffusivity (0.202 $cm^2 \cdot s^{-1}$ [31]). More recently, in the case of TiO_2 and Fe_2O_3, Laachachi et al. [4] attributed the differences observed in terms of time-to-ignition to the intrinsic thermal diffusivity of these oxides. Nevertheless, since α_{TiO2} and α_{Al2O3} are close ($\alpha_{TiO2} = 1.96 \times 10^{-6}$ $m^2 \cdot s^{-1}$, $\alpha_{Al2O3} = 1.93 \times 10^{-6}$ $m^2 \cdot s^{-1}$ [32–34]), these authors underlined the influence of an additional physico-chemical process. In their semi-crystalline system polypropylene/multi-walled nanotubes (PP/MWNT), Kashiwagi et al. [35] also observed that the thermal conductivity of their nanocomposites is higher than that of pure PP.

5.5. Discussion

We will now try to search relationships that may exist between thermal diffusivity and thermal stability, on the one hand, and some fire-retardant properties on the other hand.

As the difference in performance between nanofillers in terms of thermal diffusivity was visible in poly(methyl methacrylate) only from 10 wt% onwards, we only compared the curves obtained by thermogravimetric analysis (TGA) for PMMA, PMMA–15%Al_2O_3 and PMMA–15%TiO_2 (Fig. 13a).

These measurements show, beside the fact that adding 15 wt% metal oxide led to a significant stability enhancement of PMMA, that 15 wt% TiO_2 brought a supplementary-temperature shift of about 25 °C at half degradation compared to PMMA–15%Al_2O_3. Some of the known reasons of the improvement of thermal stability when metallic oxides are added to PMMA are clearly exposed in a previous paper [15]. The rate of thermal decomposition can be influenced by: (i) chemical parameters (molecular weight, cross-linking…); (ii) physical parameters (viscosity, compactness, heating rate, temperature gradient, thermal diffusivity…). The temperature shift of the decomposition may be indeed due to the intrinsic temperature gradient in the samples: the higher the gradient, the longer time it takes for the heat to reach the core of the sample leading in a more increasing surface temperature which undergoes a faster decomposition. Thermal diffusivity directly influences thermal gradients: the higher it is, the less time it takes for the heat to pass through the material, therefore the thermal gradient between the two sides of the sample is getting lower and finally less heat builds up on the surface slowing down the decomposition. Therefore, although the alumina used has a surface area twice as large as titanium dioxide, the higher thermal diffusivity of the latter (Fig. 13b) leads to an increase of thermal stability of its composites (Fig. 13a). So the material is less flammable resulting in an increase of the time-to-ignition (TTI). This was observed for all our nanocomposites (Fig. 14): the TTI of PMMA filled with 15% TiO_2 was increased by 25% compared to pure PMMA (increase of 22% for the same amount Al_2O_3 and AlOOH), contrary to the results obtained by Kashiwagi et al. [35] in PP/MWNT system where they observed a decrease of TTI in spite of an increase of thermal conductivity. In spite of the number of samples studied, the correlation between TTI and thermal diffusivity could not be clearly established. Further samples need to be studied.

In order to highlight possible relationships between fire-retardancy data and thermal diffusivity, THR and pHRR were plotted versus thermal diffusivity at 25 °C and at 170 °C. The trend at 25 °C is similar to the one observed at 170 °C when using thermal diffusivity data. Figs. 15 and 16 present these relationships at 25 °C. We are aware that we compare two types of data (THR, pHRR versus α) not measured in the same temperature range. Due to its

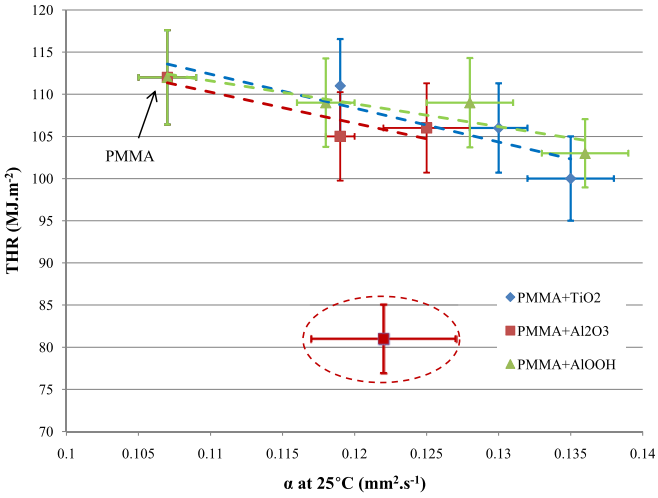

Fig. 15. THR versus thermal diffusivity α at 25 °C for PMMA, PMMA–TiO_2, Al_2O_3 and AlOOH nanocomposites.

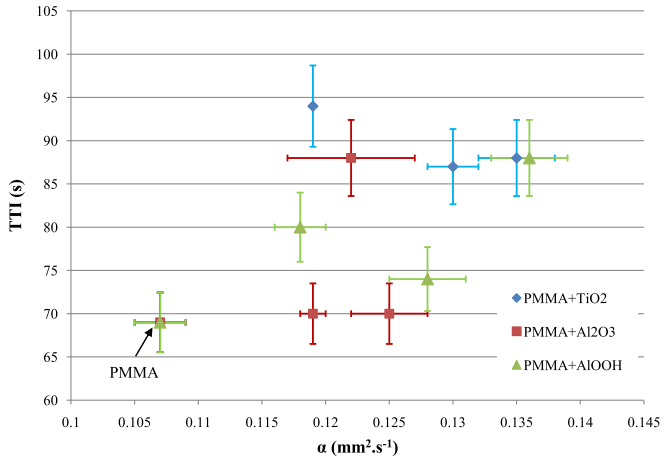

Fig. 14. TTI versus thermal diffusivity α at 25 °C for PMMA, PMMA–TiO_2, Al_2O_3 and AlOOH nanocomposites.

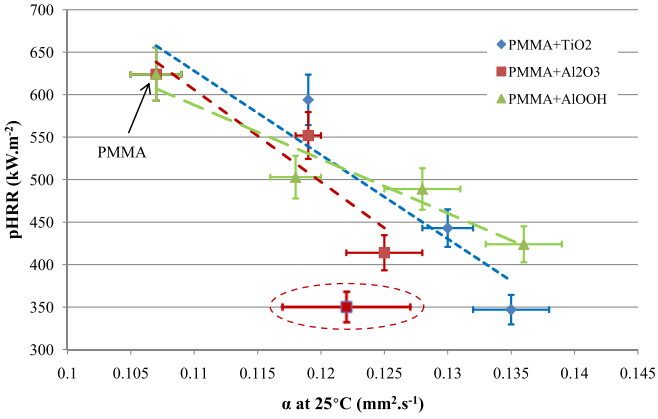

Fig. 16. pHRR versus thermal diffusivity α at 25 °C for PMMA, PMMA–TiO_2, Al_2O_3 and AlOOH nanocomposites.

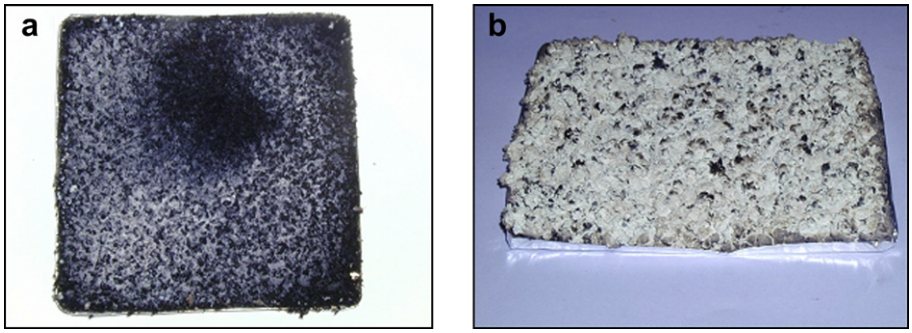

Fig. 17. Photographs after cone calorimeter tests: (a) PMMA + 15% Al_2O_3 after complete combustion [25], (b) PMMA + 15% TiO_2 after complete combustion [3].

design, the Laser Flash Analysis cannot provide measurements during the sample's degradation, and at the present time, no other method could be found in the literature for measuring thermal diffusivity of PMMA beyond its melting temperature.

Total heat release (THR) diminishes steadily as thermal diffusivity increases. Good linear correlation coefficients (R^2) were obtained for PMMA–TiO_2 and PMMA–AlOOH: respectively 0.81 and 0.83 indicating that THR seems to be somewhat related to thermal diffusivity. In fact, for each loading, data are not very different when taking into account standard deviations, except for 15 wt% alumina whose values are largely out of the range (dashed circle). That composition has indeed the lowest THR and thermal diffusivity compared to the other nanofillers studied, implying that other phenomena have to be considered for explaining the data obtained in this case.

Fig. 16 displays pHRR versus thermal diffusivity at 25 °C.

The decrease in pHRR follows a linear trend regardless of the type of filler. The linear correlation coefficient (R^2) for PMMA–TiO_2 and AlOOH (respectively 0.89 and 0.92) indicate that pHRR can also be related to thermal diffusivity. This relationship is not as strong for PMMA–Al_2O_3 due to the results obtained at 15 wt%. This confirms that other parameters have to be taken into account to explain the behaviour of this particular composition.

Indeed, at the maximum loading (15 wt%), thermal diffusivity and pHRR are the lowest, except for PMMA–15% Al_2O_3, which has a thermal diffusivity similar to PMMA–10% Al_2O_3 taking into account the standard deviations, whereas the value of pHRR is much lower at 15 wt% than at 10 wt%. The peculiar character of PMMA–15% Al_2O_3, highlighted in Figs. 15 and 16 is probably due to a higher char formation for this sample compared to other systems (Fig. 17). The formation of char during combustion probably results of the existence of a strong oxide/polymer interaction.

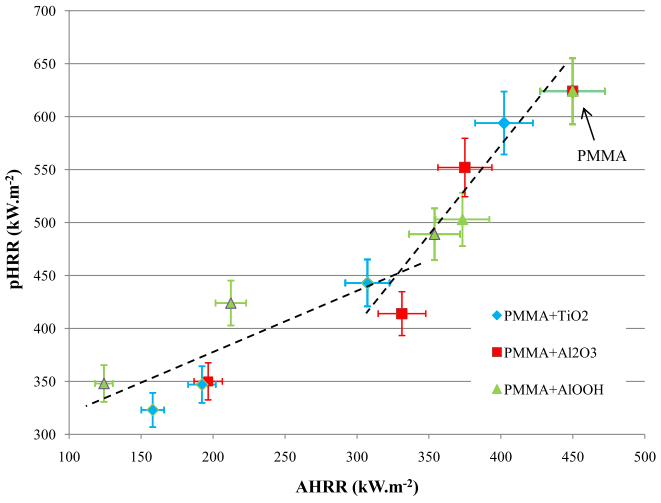

Fig. 18. pHRR versus THR for PMMA–TiO_2 and AlOOH.

THR and pHRR decrease linearly with α for all nanocomposites studied based on metal oxides (except for the alumina maximum loading which is systematically out of range). To eliminate the additional influence of the charring effect observed with Al_2O_3, pHRR values were plotted against the average heat release rate (AHRR) for all nanocomposites (Fig. 18). The AHRR corresponds to the ratio of THR and time of combustion.

A quasi bi-linear relationship between pHRR and AHRR can be seen typical of the appearance of the barrier effect from a certain nanofiller loading (about 10 wt%) for all metal oxides studied. Below 10 wt% of filler, pHHR and AHRR rise more rapidly than above. This means that the release rate of flammable volatiles is substantially higher than for composites containing 15 to 20 wt% nanofiller. This behaviour was also found by Mouritz et al. for a broad range of polymers and some composites [36].

6. Conclusions

PMMA–TiO_2, PMMA–Al_2O_3 and PMMA–AlOOH nanocomposites were prepared by melt-blending with different loadings. Relevant fire-retardant properties were achieved by adding high filler content (15 wt%). Possible relationships between flame-retardant and thermal properties (i.e., thermal diffusivity) are proposed for a better understanding of the mode of action of metal oxides in PMMA. Measurements made by Laser Flash Analysis showed that titanium dioxide and boehmite dissipate heat better than alumina, despite the fact that it has the largest surface area. Differences between nanofillers were only visible from 10 wt%. Time-to-ignition could be linked to thermal stability and diffusivity. THR and pHRR decrease linearly with α for TiO_2, Al_2O_3 and AlOOH, proving that THR and pHRR have a possible relationship with thermal diffusivity. The effect of charring is clearly demonstrated with PMMA containing 15 wt% of alumina. A bi-linear relationship was established between pHRR and AHRR showing the appearance of a barrier effect of oxide particles.

Mechanical properties of PMMA nanocomposites were shown to be significantly altered by high loadings. The evolution of the Young's modulus was attributed to the simultaneous effect of a low density interphase surrounding the oxide particles and of the increase of Tg counterbalancing the action of the interphase from 10 wt% of filler.

Acknowledgements

The authors gratefully acknowledge the financial support of the Fonds National de la Recherche (FNR) from Luxembourg. Evonik-

Degussa is acknowledged for donating TiO_2 and Al_2O_3 and Nabaltec for donating AlOOH.

References

[1] www.cefic-efra.org.
[2] Sahoo PK, Samal R. Polym Degrad Stab 2007;92(9):1700–7.
[3] Laachachi A, Leroy E, Cochez M, Ferriol M, Lopez Cuesta JM. Polym Degrad Stab 2005;89(2):344–52.
[4] Laachachi A, Cochez M, Ferriol M, Lopez Cuesta JM, Leroy E. Mater Lett 2005;59(1):36–9.
[5] Laachachi A, Cochez M, Ferriol M, Leroy E, Lopez Cuesta JM, Oget N. Polym Degrad Stab 2004;85(1):641–6.
[6] Laachachi A, Cochez M, Leroy E, Gaudon P, Ferriol M, Lopez Cuesta JM. Polym Adv Technol 2006;17(4):327–34.
[7] Parker WJ, Jenkins RJ, Butler CP, Abbot GL. J Appl Phys 1961;32(9):1679–84.
[8] Min S, Blumm J, Lindemann A. Thermochim Acta 2007;455(1–2):46–9.
[9] Blumm J, Lindemann A, Min S. Thermochim Acta 2007;455(1–2):26–9.
[10] Huggett C. Fire Mater 1980;4(2):62–5.
[11] Shenoy AV. Rheology of filled polymer systems. Dordrecht, Boston, London: Kluwer Academic Publishers; 1999. p. 16–20.
[12] Jordan J, Jacob KI, Tannenbaum R, Sharaf MA, Jasiuk I. Mater Sci Eng A 2005;393(1–2):1–11.
[13] Ash BJ, Rogers DF, Wiegand CJ, Schadler LS, Siegel RW, Benicewicz BC, et al. Polym Compos 2002;23(6):1014–25.
[14] Zulfiqar S, Masud K. Polym Degrad Stab 2002;78(2):305–13.
[15] Laachachi A, Ferriol M, Cochez M, Ruch D, Lopez-Cuesta JM. Polym Degrad Stab 2008;93(6):1131–7.
[16] Chan CM, Wu J, Li JX, Cheung YK. Polymer 2002;43(10):2981–92.
[17] Gersappe D. Phys Rev Lett 2002;89(5). 058301/1–4.
[18] Ramanathan T, Stankovich S, Dikin DA, Liu H, Shen H, Nguyen ST, et al. J Polym Sci Part B: Polym Phys 2007;45(15):2097–112.
[19] Ciprari D, Jacob K, Tannenbaum R. Macromolecules 2006;39(19):6565–73.
[20] Tannenbaum R, Zubris M, David K, Ciprari D, Jacob K, Jasiuk I, et al. J Phys Chem B 2006;110(5):2227–32.
[21] Babrauskas V, Peacock RD. Fire Saf J 1992;18(3):255–72.
[22] Gilman JW, Jackson CL, Morgan AB, Harris Jr R, Manias E, Giannelis EP, et al. Chem Mater 2000;12(7):1866–73.
[23] Gilman JW. Appl Clay Sci 1999;15(1–2):31–49.
[24] Brossas J. Techniques de l'ingénieur 1999;A3(237):1–14.
[25] Laachachi A, Ferriol M, Cochez M, Lopez Cuesta JM, Ruch D. Polym Degrad Stab 2009;94(9):1373–8.
[26] Nunes dos Santos W, Mummery P, Wallwork A. Polym Test 2005;24 (5):628–34.
[27] Chung DDL. Appl Therm Eng 2001;21(16):1593–605.
[28] Droval G. Improvement of thermal conductivity in polymer composites, http://g.droval.free.fr; 2006.
[29] Oskotsky VS, Smirnov IA. The defects in crystals and heat conduction. Leningrad: Nauka; 1972.
[30] Bashirov AB, Shermergor TD. Polym Mech 1975;11(3):474–6.
[31] www.pmmh.espci.fr/fr/Enseignement/Archives/Cours/annexes.pdf.
[32] Chase MW. NIST-JANAF thermochemical tables, 4th ed. J Phys Chem Ref Data Monograph No 9, 1998.
[33] Shackelford JF, Alexander W. Materials science and engineering handbook. Boca Raton, USA: CRC Press; 2000.
[34] Jahromi SAJ, Ali Pour MM, Beirami A. Eng Fail Anal 2003;10(4):405–21.
[35] Kashiwagi T, Grulke E, Hilding J, Groth K, Harris R, Butler K, et al. Polymer 2004;45(12):4227–39.
[36] Mouritz AP, Mathys Z, Gibson AG. Compos Part A: Appl Sci Manuf 2006;37 (7):1040–54.